16th ICAAR LISBOA 2020-2022

16th International Conference on
Alkali-Aggregate Reaction in Concrete
Lisboa | LNEC | Portugal | 31 May - 2 June 2022

http://icaar2020-2022.lnec.pt

Scale-dependent expansions of cubic mortars due to alkali silica reaction under different alkali supply conditions

Yuya Takahashi[(1)], Xi Ji[(2)], Koichi Maekawa[(3)]

(1) Department of Civil Engineering, The University of Tokyo, Tokyo, Japan, takahashi@concrete.t.u-tokyo.ac.jp

(2) Department of Civil Engineering, The University of Tokyo, Tokyo, Japan, ji@concrete.t.u-tokyo.ac.jp

(n) Department of Civil Engineering, Yokohama National University, Kanagawa, Japan, maekawa-koichi-tn@ynu.ac.jp

Abstract

This study investigates the scale dependency of expansion due to the alkali silica reaction (ASR) under various alkali supply conditions. Cubic mortar specimens of different sizes, i.e., 10, 20, 40, and 100 mm edge length, were used. Different alkali supply conditions, such as alkali leaching, alkali wrapping, and alkali supply, were prepared, and the ASRs of the mortar specimens were accelerated. The expansion progress of the prepared samples was measured through image analysis, and clear scale dependencies in ASR expansion were observed for all alkali supply conditions. Under alkali leaching, the expansion progress of smaller specimens stagnated at an early age, leading to a scale dependency. Alkali leaching can be the dominant factor for the scale dependency of the expansion. Under alkali supply, mass change during ASR acceleration was also observed. The smaller specimens showed rapid mass gains at the initial stage, followed by mass reductions at later material stages. Moreover, ASR gel exudation should govern the expansion curve under alkali supply conditions, which also causes a scale dependency. To understand the scale dependency in ASR expansion and to ensure effective expansion predictions, both alkali leaching and ASR gel movement should be considered.

Keywords: *alkali-silica reaction; expansion; scale dependency; alkali supply condition.*

1. INTRODUCTION

The alkali silica reaction (ASR) is the reaction between dissolved silica from aggregates and hydroxide ions from pore solutions containing alkalis and calcium. The ASR is one of the major deterioration phenomena in concrete, causing expansions and cracks in concrete, which can lead to excessive deformation and/or loss of mechanical performance. Research on ASR was started by Stanton in the 1940s [1], and numerous studies on the mechanisms of ASR have been conducted to date. Such works have been summarised by Rajabipour et al. and other researchers [2-4]. Many factors including the specimen size, can influence the expansion progresses by ASR [2,4]. Several researchers have pointed out the scale dependency of ASR expansion experimentally [5-7], and the main factor is supposed to be alkali leaching from the specimens. Recently, Multon and Sellier [8] employed modelling approaches to explain ASR expansion progress based on the chemical and physical coupling model. They proposed that the additional factors should be fracture mechanics [5] and ASR gel exudation from specimens [7-9]. ASR gel exudation can be observed experimentally [10], but its effect on the scale has not yet been discussed in detail. With highly reactive aggregates, ASR gels with low viscosity and stiffness can be generated rapidly [11,12] and flow out from the aggregate into the existing cracks [13].

Alkali supply conditions during ASR acceleration are pertinent to the scale effect. However, in previous studies, the experiments were conducted mostly in the single alkali supply conditions, including moist cloth wrapping in the study by Takahashi et al. [7], and alkali solution immersion in the study by Gao et al. [5]. The effect of alkali supply conditions on the scale dependency of the ASR expansion should be thoroughly investigated. For measurement, the prism-shaped specimens were mainly used to measure the expansion by strain gauge or other methods. This can measure expansions only in the longitudinal directions of prism specimens. The three-dimensional effect cannot be neglected in the experiments. In

this study, ASR acceleration experiments with different sizes and alkali supply conditions were conducted on cubic specimens to determine the cause of the scale dependency in ASR.

2. EXPERIMENTAL PROGRAM

2.1 Specimen Preparation

Cubic mortar specimens were fabricated with reactive aggregates, and their accelerated ASR expansion progress was measured. Two different reactive aggregates, S1 and S2, were used as fine aggregates. S1 and S2 were from the Hokuriku and Hokkaido regions of Japan, respectively. The petrological components and properties of the aggregates are shown in Tables 2.1 and 2.2, respectively. Based on this information, aggregate S2 can be regarded as more reactive than S1 for ASR. Ordinary Portland cement with an alkali content (Na_2O_{eq}) of 0.59 wt% (Na_2O: 0.33%; K_2O: 0.39%) and a density of 3.15 kg/m^3 was used. Cubic mortar specimens with different sizes (100, 40, 20, and 10 mm, Figure 2.1) were made with the mix proportions listed in Table 2.3. Further, 100% of S1 and S2 were used as fine aggregates for mix proportions I and II, respectively. The water-to-cement ratio of the specimens was set to 0.5, and NaOH was added to accelerate the ASR. In the authors' previous numerical study [7], the possible ASR gel migration distance can be several millimetres to several centimetres. Hence, 10 mm to 100 mm was set as the specimen size, and the cube shape was selected to disregard the three-dimensional shape effect on expansion.

Table 2.1: Petrological components of aggregates

	Ratio [%]						
	Andesite**	Rhyolite*	Welded tuff**	Granite	Diorite	Sandstone	Shale*
S1	45.2	1.7	23.4	23.1	5.2	1.0	0.5
S2	100.0	-	-	-	-	-	-

**Highly reactive rock types, *Reactive rock types

Table 2.2: Properties of reactive aggregates

	Density (kg/m^3)	Test with JIS A 1145 (Chemical method)		Test with JIS A 1146 (Mortar bar test)
		Dissolved silica, Sc	Alkali reduction, Rc	Expansion
S1	2.58	166 mmol/l	156 mmol/l	0.047% at 3 months 0.051% at 6 months
S2	2.70	624 mmol/l	111 mmol/l	0.433% at 3 months 0.461% at 6 months

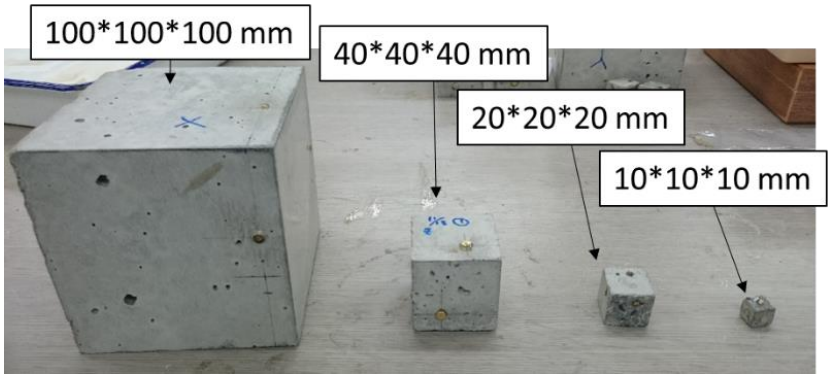

Figure 2.1: Cubic mortar specimens of different sizes

Table 2.3: Mix proportions

	Unit Weight (kg/m^3)				
	Water	Cement	S1	S2	NaOH
I	296	591	1331	0	11.61
II	303	605	0	1362	11.89

Three different ASR acceleration conditions were prepared: (1) “WW” (water wrapping), (2) “AW” (alkali wrapping), and (3) “AS” (alkali solution). A general timeline for each condition is presented in Table 2.4. Sufficient water was supplied under all conditions, while the alkali supply conditions were different. The specimens in the WW condition were wrapped with gauze wetted with pure water and with thin plastic films (similar to the general protocols of RILEM AAR-3/AAR-4) after 16 days of sealed curing; subsequently, they were stored in an environmental control chamber at 40 °C (Figure 2.2). Further, water was added to the clothes at each measurement time to maintain sufficiently wet conditions. Under these conditions, the alkalis in the pore water could easily leach out from the specimens. Specimens at condition AW were accelerated with the alkali-wrapping method proposed by Kawabata et al. [14], which has also been adopted in other studies [15]. The general protocols are nearly identical to those of RILEM AAR-3/AAR-4, with the only difference being the wrapping of concrete specimens with a wet cloth containing NaOH solution. After 10 days of sealed curing, the mortar specimens were wrapped with polypropylene non-woven cloth of the size given in Table 2.5. Based on a method proposed in previous studies [16,17], the alkali concentration in pore water was assumed to be 1.6 mol/L; hence, a 1.6 mol/L NaOH solution was added to the clothes at 0.039 g/(cm^2 of the area of cloth). Subsequently, the specimens were wrapped in thin plastic film and stored at 40 °C. The weights of the clothes were measured at the time of expansion measurement, and the same weight of pure water was added to the clothes. At this time, no additional alkali was supplied, and only pure water was added. With this treatment, the alkali elution from or supply to the specimen was controlled to be reduced under the AW condition. The specimens under AS condition were soaked in 1.6 mol/L NaOH solution after 10 days of sealed curing and kept at 40 °C. Under these conditions, sufficient additional alkali can be supplied to the specimen during the ASR acceleration.

Table 2.4: ASR acceleration conditions

WW	Alkali leaching condition (Water wrapping)	16 days sealing (20 °C constant) → Wrapped with a wet cloth and sealed with a plastic film → 40 °C constant
AW	Alkali wrapping condition	10 days sealing (20 °C constant) → Wrapped with clothe wet with 1.6 mol/l NaOH solution and sealed with a plastic film → 40 °C constant
AS	Alkali supply condition	10 days sealing (20 °C constant) → soaked in 1.6 mol/l NaOH solution (40 °C constant)

Figure 2.2: Water wrapping of specimen

Table 2.5: Sizes of clothes for condition AW

Size of specimen (mm)	100	40	20	10
Size of cloth (mm^2)	217800	54450	13613	3428

Table 2.6 shows the test series in this study. With mix proportion I (with aggregate S1), expansion progresses with different ASR acceleration conditions (WW, AW, and AS) were compared. With ASR acceleration condition AS, expansion progresses with different reactive aggregates (S1 and S2) can be compared. Three specimens with each size are made for the experimental series. The weight change over the experimental program was monitored to indicate how fairly the specimens were sealed on vapor and ions for WW and AW conditions and was controlled within 0.1% of the accuracy limit of the measurement device.

Table 2.6: Experimental series

Series	Mix proportion	ASR acceleration condition	Sizes of the specimens
I-WW [7]	I	WW	100, 40, 20 and 10 mm
I-AW	I	AW	100, 40, 20 and 10 mm
I-AS	I	AS	100, 40 and 20 mm
II-AS	II	AS	100, 40 and 20 mm

2.2 Measurement procedures

Since some of the specimens used in this experiment were smaller than the standardised dimensions and the environmental conditions were quite humid, length change measurements with existing embedded or surface strain gauges could not be conducted for the smaller specimens. An image-scanning method was adopted to measure the expansion progress. A 3D shape-measuring machine (KEYENCE, VR-3100, Figure 2.3) was employed for the measurements. Two feature points on certain surfaces were predesignated, and the distance between them was measured throughout the test period (Figure 2.4). The minimum error of the measurement instrument was ~2 μm. It took 1-2 minutes for each measurement. The accuracy of this measurement method was confirmed with the strain gauge method applied to a 100 mm cube specimen in a previous study [7]. Two surfaces of each specimen were selected for continuous measurements. There were three specimens; thus, a total of six lengths were measured for each specimen size in each experimental series. Herein, the average of the six measurements is displayed. The measurements were conducted thrice on each surface, and the average of the three measurements was taken as the final value. To eliminate the effect of thermal expansion and shrinkage, the specimens were held at 20 °C for 2.5 hours for cooling by keeping the entire sheet wrapped before measuring the length change. To prevent drying, the specimens in the AS condition were wrapped with plastic film during cooling. During measurement, including measurement preparatory work, the specimens were inevitably exposed to ambient conditions, as shown in Figure 2.3. Short-term drying in small ranges may not be avoided, even though each measurement took approximately 20 min. In the preliminary test, the length change during the measurement was controlled within 50-100 μm/m. This is within the range of limit accuracy for the measuring device and within 10% of the overall volumetric deformation. The base zero lengths were measured after sealed curing, and the calculated expansion strains were compared for different specimen sizes and test series. The masses of the I-AW, I-AS and II-AS specimens were continuously measured throughout the ASR acceleration period.

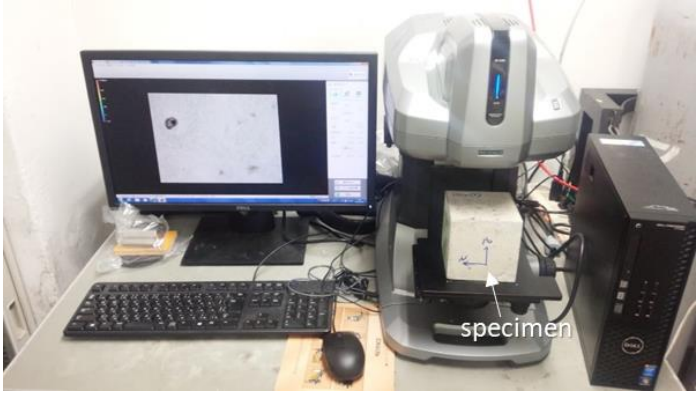

Figure 2.3: 3D shape measurement equipment

Figure 2.4: Example of image scanning method for length measurements

For the first 400 days of material aging, the expansions were measured at intervals of several days to several weeks. After 400 days, 20 mm, 40 mm, and 100 mm specimens of the I-AW, I-AS, and II-AS series were stored continuously under the designated storage conditions shown in Table 2.4. After approximately 1000 days of material aging, the expansions were measured again.

After the final expansion measurement, X-ray computed tomography (X-ray CT) measurements were conducted on the 20 mm cubic specimen of the II-AS series to determine the internal crack distribution. A ScanXmate-D200RSS900 was used for the scanning. The scanned images, with a resolution of 21 μm, were processed with an unsharp mask filter, and the phases were classified using the Trainable Weka Segmentation method [18] to separate the air voids and cracks. Air voids were eliminated from the phases for visualisation, and only the crack phases were classified using the total voxel numbers for visualisation. The voxel size of the analyses is 9.3E+3 μm^3.

3. RESULTS AND DISCUSSION

3.1 Expansion strains and mass changes

Figures 3.1 and 3.2 show the measured expansion progressed until 400 days of material age for I-WW and I-AW, respectively. For these cases, the levels of expansion were higher, in the order of 100, 40, and 20 mm, showing a clear dependence on the size. This could be because, the smaller the size, the larger the specific surface area, the greater the amount of alkali elution, and the easier it is for the gel to exude. The I-WW series has a larger effect of alkali leaching, which leads to a larger size dependency in the expansion progress. Meanwhile, the expansions were almost the same for the 10 mm and 20 mm specimens, indicating the influence of the larger specific surface area and larger water supply for the 10 mm specimen. Figure 3.3 shows the measured mass change of the I-AW series during expansion. The smaller specimens have a rapid mass increase at the initial acceleration stage, which leads to a fast rate of expansion progress at the initial stage. Upon focusing on the 10 mm specimen, a mass decrease can be observed after a mass increase in the first 15 days of acceleration. This could be due to ASR-gel exudation from the surface.

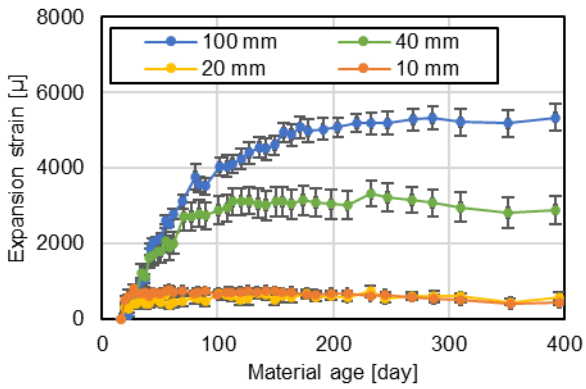

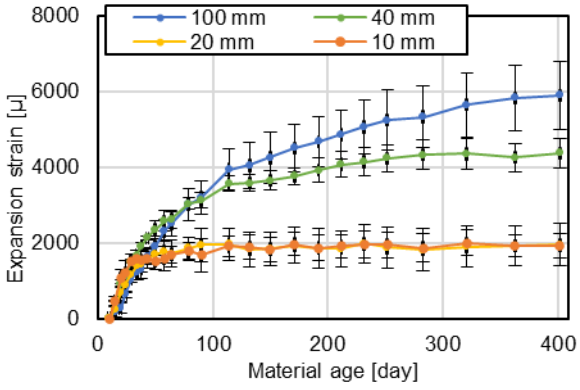

Figure 3.1: Expansion progresses of I-WW series [7] Figure 3.2: Expansion progress of I-AW series

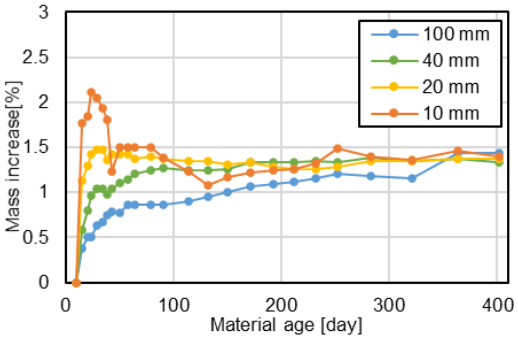

Figure 3.3: Mass change of I-AW series

Figures 3.4 and 3.5 show the measured expansion progresses until 400 days of material age for I-WW and I-AW, respectively. The I-AS and II-AS series had alkali-supply conditions and showed a larger expansion rate than the other environments. Moreover, the final expansion levels were much larger than those in the other environments, because of the high alkali supply during the acceleration period in 1.6 mol/L NaOH solution. The 40 mm specimens showed a larger expansion than the 20 mm specimens. This observation was similar to the other conditions (WW and AW). However, the 100 mm specimens showed a slightly different tendency, by exhibiting the largest expansion amount at the end of the measurement, while the start of expansion was slow. Thus, it can be said that the smaller the specimen, the faster the alkali and water supply, and thus, the greater the expansion speed in the initial stage. In the later stage of expansion, the larger specimens have larger expansion even if they have less alkali and water supply, owing to the smaller surface area. The larger specimen had less ASR gel exudation, owing to the long distance from the internal part of the specimen to the surface, which can be the main cause of greater expansion at a later stage. This type of scale dependency in alkali supply conditions was also observed in a previous study by Gao et al. [5].

Figures 3.6 and 3.7 show the measured mass changes of the I-AS and II-AS series, respectively. In the initial stage of acceleration, a large mass gain was observed in the smaller specimens, similar to that in the I-AW series. This indicates that the rates of alkali and water supply were relatively higher for small specimens. Subsequently, mass loss was observed in some of the specimens. During this period, no clear loss of pieces from the specimens was observed, and this mass loss could be due to gel exudation. The smaller the specimen, the larger the mass loss, suggesting that the amount of expansion is suppressed by gel exudation. In addition, the mass loss was larger in the II-AS series using highly reactive aggregates. The physical properties of the generated gel differ because of the difference in the reaction rate. The gel exudation rate from the specimen surface is thought to be different, owing to aggregate reactivity.

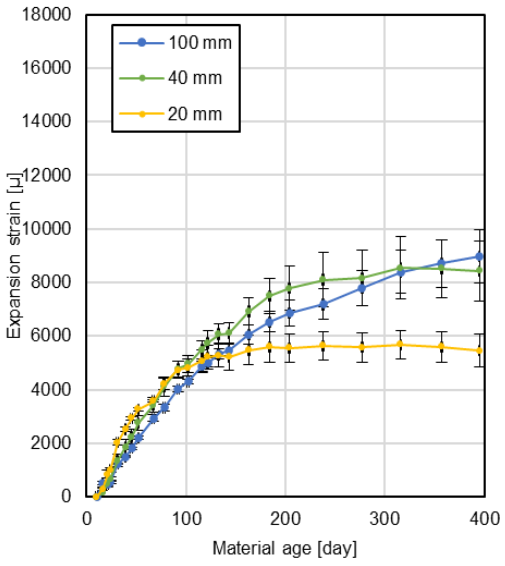

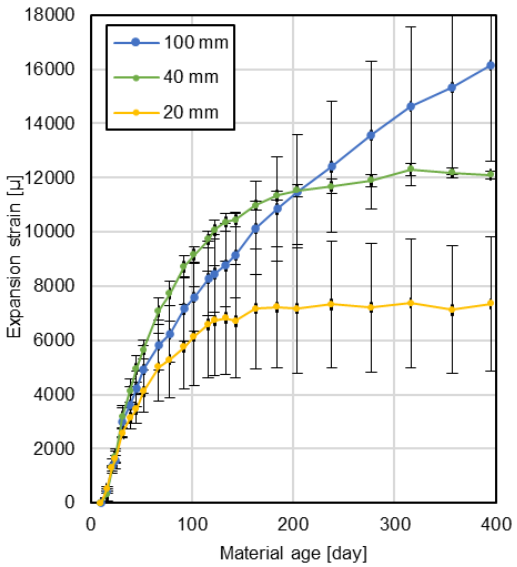

Figure 3.4: Expansion progresses of I-AS series Figure 3.5: Expansion progresses of II-AS series

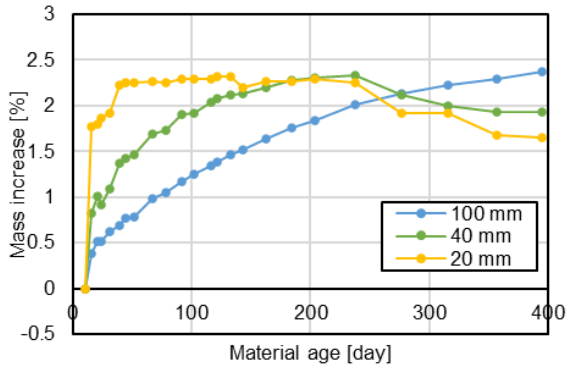

Figure 3.6: Mass change of I-AS series

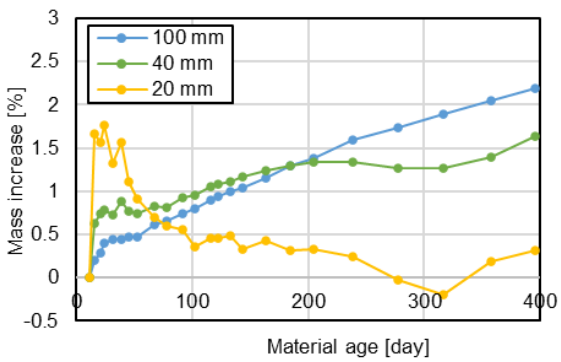

Figure 3.7: Mass change of II-AS series

After 400-day measurements, 20 mm, 40 mm, and 100 mm specimens of the I-AW, I-AS, and II-AS series were continuously stored under the designated storage conditions specified in Table 2.4, until after 1000 days, and then the expansions were measured again. Figure 3.8 shows a comparison of the expansion strain between approximately 400 and 1000 days. The scale dependency of the ASR expansion prevailed even after 1000 days in all cases. It can be said that the final expansion level can vary for different specimen sizes. The difference between the 40 and 100 mm specimen of the I-AS series was not clear at 400 days, as shown in Figure 3.4. However, it became clearer after 1025 days. For the 20 and 40 mm specimens of the I-AS series, the expansion strains decreased from 400-days to 1000-days. For these specimens, expansions are already stable before 400 days, and this decrease in expansion can be caused by ASR gel exudation from the surface.

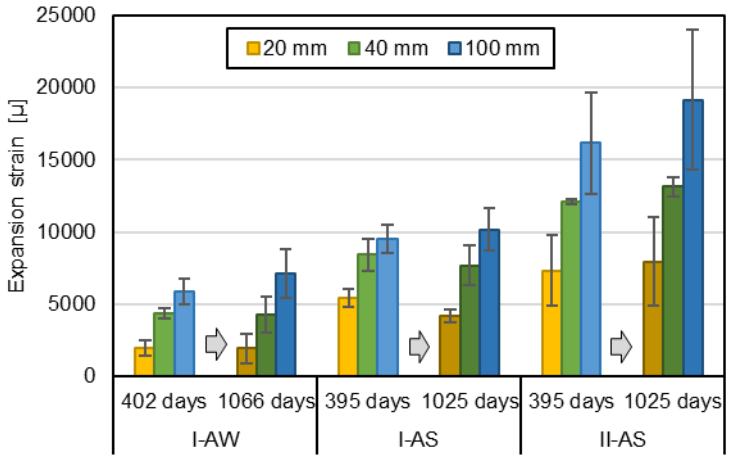

Figure 3.8: Expansion measurements after 1000 days

3.2 Crack observations

The scanned images for the length measurements of II-AS are shown in Figure 3.9. Surface crack propagation with increasing material age can be observed in these images. Major cracks already appeared at 67-day measurements with 20 mm and 40 mm specimens, whereas they gradually appeared around 117 days in the 100 mm specimen. As shown in Figure 3.5, the expansion strains of these cases are almost in the same range until several dozens of days, however, the crack appearances are different. Gao et al. [5] pointed out that a larger aggregate-to-specimen size ratio can cause faster cracking around the aggregate, considering the fracture mechanics. In this study, the relationships among scale dependency, aggregate size, and cracking behaviour could not be examined in depth; this limitation can be addressed in a future study.

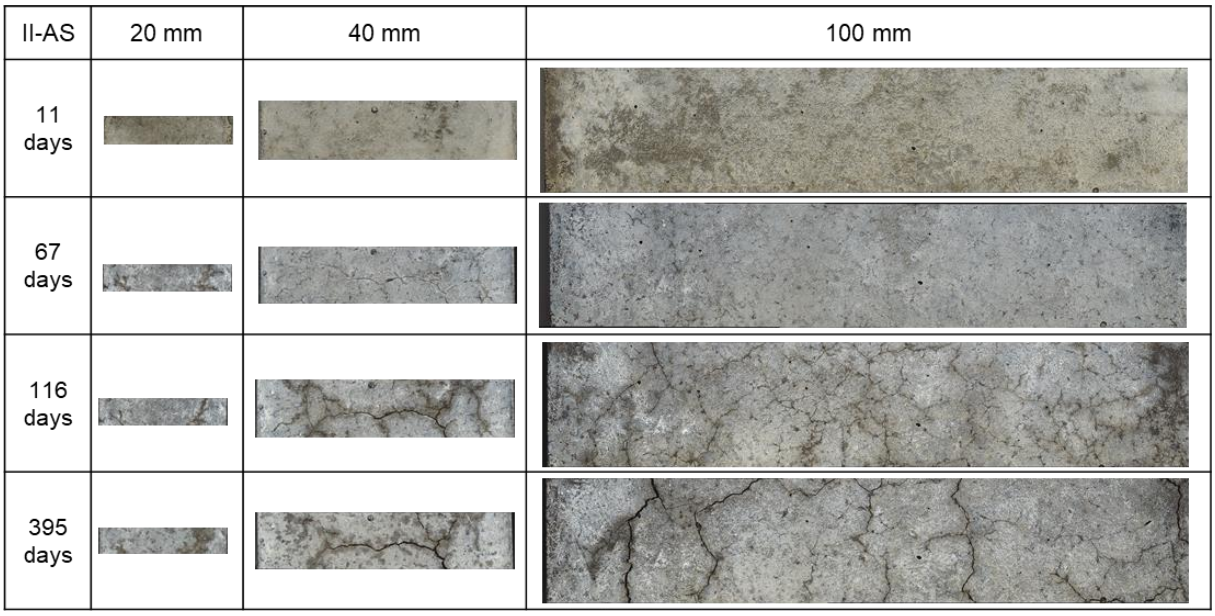

Figure 3.9: Scanned images for length measurements for II-AS series

To determine the internal crack distributions after ASR expansion, X-ray CT measurements were conducted for 20 mm specimen of the II-AS series after 1000-days of expansion measurement. Figure 3.10 shows the internal crack distributions visualised from the X-ray CT measurement results. Among the detected cracks, the connected cracks with total voxel numbers of 500–2000 are grey, while the connected cracks with more than 2000 voxels are orange. The crack width distributions for each connected crack size are shown in Figure 3.9. In the specimen, a few penetrated cracks were observed, and some of the cracks were larger than 0.1 mm. Whereas, other tiny cracks were distributed over the entire specimen. In this study, only one specimen (a 20 mm specimen of the II-AS series) was measured using X-ray CT. After the measurements of other specimens, the relationships between the scale effect and crack behaviour can be studied and discussed in the future.

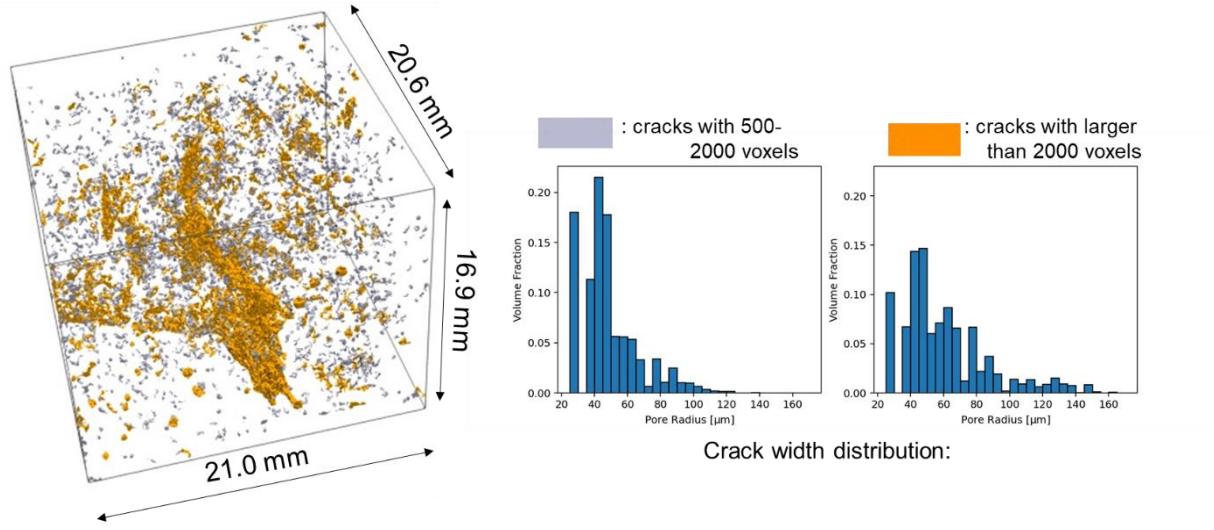

Figure 3.10: X-ray CT results for II-AS 20 mm specimen

4. CONCLUSIONS

In this study, the ASR expansion progress of cubic mortar specimens of different sizes was measured under different alkali supply environment conditions. Various expansion trends consistent with different alkali supply conditions were observed, and scale dependencies were examined in all conditions, with

larger specimens showing greater expansion. Through observation of the mass transition along with the expansion transition, it was shown that water and alkali supply was dominant in the early stage, which led to rapid expansion progress with smaller specimens. Whereas, the ASR gel exudation was dominant in the later stage, which led to higher final expansion levels for larger specimens. To understand the ASR expansion behaviour, not only the alkali supply/leaching effect but also the gel movement effect should be properly considered. In the future, the relationship between scale dependency and crack progress behaviour should be studied further.

5. ACKNOWLEDGEMENTS

This study was financially supported by the JSPS KAKENHI 18H01507 and 21H01416. We are grateful to Shimpei Ogawa, Yuichiro Tanaka, and Izuru Segawa from the University of Tokyo for their help in the expansion measurement conducted in this study, and Dr. Yuichiro Kawabata from the Port and Airport Research Institute for his help with X-ray CT measurements.

6. REFERENCES

[1] Stanton TE (1940) Expansion of concrete through reaction between cement and aggregate. Proc Am Soc Civ Eng 66:781–1812.

[2] Rajabipour F, Giannini E, Dunant C, Ideker JH, Thomas MDA (2015) Alkali-silica reaction: Current understanding of the reaction mechanisms and the knowledge gaps. Cem Concr Res 76:130–146. https://doi.org/10.1016/j.cemconres.2015.05.024.

[3] Sims I, Poole AB (2017) Alkali-Aggregate Reaction in Concrete: A World Review, CRC Press.

[4] Lindgård J, Andiç-çak Ö, Fernandes I, Rønning TF, Thomas MDA (2012) Alkali – silica reactions (ASR): Literature review on parameters in fluencing laboratory performance testing. Cem Concr Res 42:223–243. https://doi.org/10.1016/j.cemconres.2011.10.004.

[5] Gao XX, Multon S, Cyr M, Sellier A (2013) Alkali-silica reaction (ASR) expansion: Pessimum effect versus scale effect. Cem Concr Res 44:25–33. https://doi.org/10.1016/j.cemconres.2012.10.015.

[6] Lindgård J, Thomas MDA, Sellevold EJ, Pedersen B, Andiç-çak Ö, Justnes H, Rønning TF (2013) Alkali–silica reaction (ASR) — performance testing: Influence of specimen pre-treatment, exposure conditions and prism size on alkali leaching and prism expansion. Cem Concr Res 53:68–90. https://doi.org/10.1016/j.cemconres.2013.05.017.

[7] Takahashi Y, Ogawa S, Tanaka Y, Maekawa K (2016) Scale-dependent ASR expansion of concrete and its prediction coupled with silica gel generation and migration. J Adv Concr Technol 14:444–463. https://doi.org/10.3151/jact.14.444.

[8] Multon S, Sellier A (2019) Expansion modelling based on cracking induced by the formation of new phases in concrete. Int J Solids Struct 160:293–306. https://doi.org/10.1016/j.ijsolstr.2018.11.001.

[9] Takahashi Y, Shibata K, Maruno M, Maekawa K (2015) Uniaxial restraint tests under high-stress conditions and a chemo-hygral model for ASR expansion. in: CONCREEP 2015 Mech Phys Creep, Shrinkage, Durab Concr Concr Struct - Proc 10th Int Conf Mech Phys Creep, Shrinkage, Durab Concr Concr Struct. https://doi.org/10.1061/9780784479346.127.

[10] Kawamura M, Iwahori K (2004) ASR gel composition and expansive pressure in mortars under restraint. Cem Concr Compos 26:47–56. https://doi.org/10.1016/S0958-9465(02)00135-X.

[11] Vayghan AG, Rajabipour F, Rosenberger JL (2016) Composition-rheology relationships in alkali-silica reaction gels and the impact on the Gel's deleterious behavior. Cem Concr Res 83:45–56. https://doi.org/10.1016/j.cemconres.2016.01.011.

[12] Okano Y, Takahashi Y (2020) Macroscale and sicroscale studies on time-dependent mechanical properties of concrete with alkali silica reactions. In: Wang C.M., Dao V., Kitipornchai S. (eds) EASEC16. Lecture Notes in Civil Engineering, 101. Springer, Singapore. https://doi.org/10.1007/978-981-15-8079-6_173

[13] Maraghechi H, Shafaatian SMH, Fischer G, Rajabipour F (2012) The role of residual cracks on alkali silica reactivity of recycled glass aggregates. Cem Concr Compos 34:41–47. https://doi.org/10.1016/j.cemconcomp.2011.07.004.

[14] Kawabata Y, Yamada K, Sagawa Y, Ogawa S (2018) Alkali-wrapped concrete prism test (AW-CPT) – New testing protocol toward a performance test against alkali-silica reaction. J Adv Concr Technol 16:441–460. https://doi.org/10.3151/jact.16.441.

[15] Kawabata Y, Dunant C, Yamada K, Scrivener K (2019) Impact of temperature on expansive behavior of concrete with a highly reactive andesite due to the alkali–silica reaction. Cem Concr Res 125:105888. https://doi.org/10.1016/j.cemconres.2019.105888.

[16] Kawabata Y, Yamada K. (2015) Evaluation of alkalinity of pore solution based on the phase composition of cement hydrates with supplementary cementitious materials and its relation to suppressing ASR expansion. J Adv Concr Technol 13:538–553. https://doi.org/10.3151/jact.13.538.

[17] Yamada K, Sagawa Y, Nagase T, Ogawa S, Kawabata Y (2016) Importance of alkali-wrapping in concrete prism tests. in: Proc. 15th Int Conf Alkali Aggreg React. Concr. P084.

[18] Arganda-Carreras I, Kaynig V, Rueden C, Eliceiri KW, Schindelin J, Cardona A, Sebastian Seung H (2017) Trainable Weka Segmentation: a machine learning tool for microscopy pixel classification. Bioinformatics 33: 2424–2426. https://doi:10.1093/bioinformatics/btx180.